Inorganic Chemistry

Article

pubs.acs.org/IC

Pyridinophane Platform for Stable Lanthanide(III) Complexation

Goretti Castro,[†] Rufina Bastida,[‡] Alejandro Macías,[‡] Paulo Pérez-Lourido,*[,†] Carlos Platas-Iglesias,*[,§] and Laura Valencia[†]

[†]Departamento de Química Inorgánica, Facultad de Ciencias, Universidade de Vigo, As Lagoas, Marcosende, 36310 Pontevedra, Spain

[‡]Departamento de Química Inorgánica, Facultad de Química, Universidad de Santiago de Compostela, Avda. de las Ciencias s/n, E-15782, Santiago de Compostela, Spain

[§]Departamento de Química Fundamental, Facultade de Ciencias, Universidade da Coruña, A Coruña, Spain

Supporting Information

ABSTRACT: A detailed investigation of the solid state and solution structures of lanthanide(III) complexes with the macrocyclic ligand 2,11,20-triaza[3.3.3](2,6)-pyridinophane (TPP) is reported. The solid state structures of 14 different Ln^{3+} complexes have been determined using X-ray crystallography. The ligand is coordinating to the Ln^{3+} ion by using its six nitrogen atoms, while nitrate or triflate anions and water molecules complete the metal coordination environments. The structure of the complexes in solution has been investigated by ^{1}H and ^{13}C NMR spectroscopy, as well as by DFT calculations (TPSSh model) performed in aqueous solution. The structures obtained from these calculations for the complexes with the lightest Ln^{3+} ions (La−Sm) are in very good agreement with those determined by the analysis of the Ln^{3+}-induced paramagnetic shifts. A structural change occurs across the lanthanide series at Sm^{3+}; the complexes of the large Ln^{3+} ions (La−Nd) are chiral due to the nonplanar conformation of the macrocycle, and present effective C_{3v} symmetries in solution as a consequence of a fast interconversion of two enantiomeric forms with C_3 symmetry. The activation free energy for this enantiomerization process, as estimated by using DFT calculations, amounts to 33.0 kJ·mol^{-1}. The TPP ligand in the complexes of the heaviest Ln^{3+} ions (Eu−Lu) presents a half-chair conformation, which results in C_s symmetries in solution.

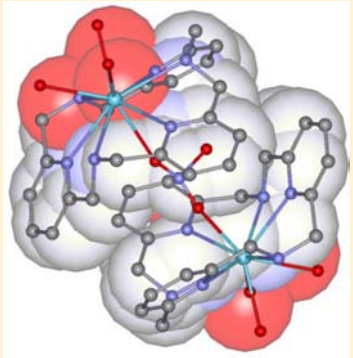

INTRODUCTION

Complexes of the trivalent lanthanide ions are useful in different medical applications that include both diagnosis and therapy.[1] Early therapeutic applications of a lanthanide included the use of cerium oxalate as an antiemetic drug.[2] Lanthanide compounds have been also tested for the treatment of tuberculosis, as anticoagulant or for the treatment of liver toxicity, antiatheroesclerosis, and rheumatoid arthritis.[3] They have found a role for the treatment of hyperphosphatemia[4] and as active agents in cancer radiotherapy.[5] Besides, photoactive lanthanide complexes show biological applications in photodynamic therapy (PDT), a noninvasive treatment modality of cancer using a photosensitizer drug and radiation.[6] However, the enormous interest devoted to lanthanide coordination chemistry in aqueous solution in the last few decades is mainly related to the successful biomedical applications of lanthanide complexes as contrast agents in magnetic resonance imaging (MRI)[7] and as luminescent probes in biomedical analysis and optical imaging.[8] MRI is a noninvasive diagnostic procedure that provides excellent quality and high resolution images. The Gd^{3+} ion, with seven unpaired electrons and favorable properties in terms of electronic relaxation, has played an important role in the revolutionary development of MRI.[9]

Ln^{3+} ions are toxic heavy metals, with a size approximating Ca^{2+} but with a higher charge, which results in a high affinity for Ca^{2+} sites in biological molecules. Indeed, Ln^{3+} ions can substitute Ca^{2+} in proteins,[10] but also other metals such as Mg^{2+}, Fe^{3+}, and Mn^{2+}.[1] Thus, complexes of the Ln^{3+} ions for biomedical applications must present high thermodynamic and kinetic stabilities to prevent the release of the toxic metal ion. The Ln^{3+} ions show a high affinity toward polyaminocarboxylate ligands, either macrocyclic or linear.[11] However, macrocyclic platforms are often preferred for biomedical applications because they provide higher thermodynamic stability and kinetic inertness.[12] Among the macrocyclic scaffolds used for stable Ln^{3+} complexation, ligands based on tetraazacyclododecane (cyclen) have been proven to be particularly useful.[7] The expanded porphyrinlike macrocycles known as Texaphyrins are large planar ligands that coordinate efficiently large cations such as the Ln^{3+} ions,[13] the corresponding complexes showing photocytotoxicity through the PDT effect.[14] Lanthanide complexes with crown ethers containing different pendant arms have been also shown to have interesting properties, but their thermodynamic stability is generally lower than that of cyclen-based analogues.[15]

Pyridinophanes such as 2,11-diaza[3.3](2,6)pyridinophane (DPP) and 2,11,20-triaza[3.3.3](2,6)pyridinophane (TPP,

Received: February 18, 2013
Published: April 29, 2013

   dx.doi.org/10.1021/ic400389d | Inorg. Chem. 2013, 52, 6062−6072

Chart 1) were first obtained following a one-pot nucleophilic condensation of 2,6-bis(chloromethyl)pyridine with TsNHNa,

Chart 1. Structure of the Ligands Discussed in This Work and Numbering Scheme Used for NMR Spectral Assignment

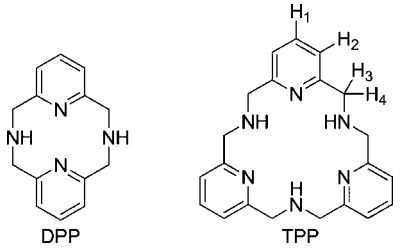

acting both as the nitrogen source and as the base, followed by the detosylation of the amine groups.[16] This procedure provides DPP as the main reaction product, which must be purified to eliminate the impurities of TPP. Alternatively, TPP was also obtained by coupling of *N,N*-bis[[6-(bromomethyl)-pyridin-2-yl]methyl]-*p*-tosylamide with tosylated 2,6-bis-(aminomethyl)pyridine.[17] DPP was shown to form unique Fe^{2+} and Co^{2+} eight-coordination complexes in which the metal ion is sandwiched by two DPP units, while Fe^{3+} and Ni^{2+} were shown to form pseudo-octahedral complexes.[18] Recently, Ln^{3+} complexes based on the DPP platform containing picolinate pendant groups have been reported.[19] However, the stability of the complexes was shown to be relatively low, which has been attributed to the small cavity of the macrocyclic fragment and the low basicity of the ligand.

We envisaged that the large macrocyclic cavity of TPP could provide a convenient platform for the design of stable Ln^{3+} complexes for biological applications. Indeed, this potentially hexadentate macrocyclic structure can be easily functionalized via alkylation of the three secondary amine nitrogen atoms. The introduction of three pendant arms containing carboxylate or phosphonate groups would result in nonadentate ligands that might leave a vacant coordination position for a water molecule, thereby providing complexes with potential application in MRI. Alternatively, the introduction of different pendant groups containing exchangeable protons could be used to obtain PARACEST agents for MRI,[20] which generate contrast by chemical exchange saturation transfer (CEST) and use a paramagnetic agent to shift the resonance of protons exchanging with bulk water protons. As a first step toward this direction, herein we investigate the coordinative properties of TPP toward the Ln^{3+} ions by using different experimental and theoretical tools. The X-ray crystal structures of 14 TPP Ln^{3+} complexes have been determined by using single-crystal X-ray crystallography. The structure and dynamics of the complexes in solution have been investigated by using ^1H NMR spectroscopy and density functional theory (DFT) calculations. An analysis of the Ln^{3+}-induced paramagnetic shifts was also carried out to determine the structure of the complexes in D_2O solution.

EXPERIMENTAL SECTION

Measurements. Infrared (IR) spectra were recorded as KBr discs on a Bruker VECTOR 22 spectrometer. ESI experiments were performed on an microTOF(focus) mass spectrometer (Bruker Daltonics, Bremen, Germany). Ions were generated using an ApolloII (ESI) source and ionization was achieved by electrospray. ^1H NMR spectra were recorded in D_2O solutions, on a Bruker ARX400 NMR spectrometer.

Materials. All chemicals used were of the highest available purity and were not purified further. Ligand TPP was synthesized as it has been reported previously.[17] Hydrated lanthanide(III) nitrates and triflates were obtained from Aldrich. Solvents used were of reagent grade and purified by usual methods.

Preparation of the Complexes. General Procedure. A solution of $Ln(NO_3)_3{\cdot}xH_2O$ or $Ln(CF_3SO_3)_3{\cdot}xH_2O$ (0.40−1.50 mmol) in methanol (5 mL) was added to a stirred solution of 0.67 equiv of TPP in the same solvent (10 mL). The addition of the metal salt led to the immediate precipitation of all complexes, except those of Nd^{3+} (**Nd-TPP**) and Lu^{3+} (**Lu-TPP**), which were soluble in methanol. The precipitate was decanted, dried, and recrystallized in water to yield the corresponding lanthanide complex.

$[(LaTPP)_2$-μ-$(NO_3)(H_2O)_6](NO_3)_5{\cdot}3.75H_2O$ (La-TPP). TPP (0.360 g, 1.00 mmol) and $La(NO_3)_3{\cdot}5H_2O$ (0.623 g, 1.50 mmol), yield: 63%. IR (KBr, cm^{-1}): 1604 (m), 1578 (m) [ν(C=C) and $\nu(C{=}N)_{py}$], 1468 (s), 1384 (s), 1314 (s), 1087 (m), 1036 (m), 791 (m), 730 (m) [$\nu(NO_3^-)$], 3296 (m), 3230 (m) [ν(NH)]. MS (ESI, *m/z*): 623 $[La(TPP)(NO_3)_2]^+$.

$[(CeTPP)_2$-μ-$(NO_3)(H_2O)_6](NO_3)_5{\cdot}3.5H_2O$ (Ce-TPP). TPP (0.151 g, 0.42 mmol) and $Ce(NO_3)_3{\cdot}6H_2O$ (0.273 g, 0.63 mmol), yield: 44%. IR (KBr, cm^{-1}): 1605 (m), 1579 (m) [ν(C=C) and $\nu(C{=}N)_{py}$], 1450 (s), 1383 (s), 1327 (s), 1087 (m), 1039 (m), 816 (m), 786 (m), 742 (m) [$\nu(NO_3^-)$], 3275 (m), 3206 (m) [ν(NH)]. MS (ESI, *m/z*): 624 $[Ce(TPP)(NO_3)_2]^+$.

$[(PrTPP)_2$-μ-$(NO_3)(H_2O)_6][Pr(NO_3)_6](NO_3)_2{\cdot}4H_2O$ (Pr-TPP). TPP (0.151 g, 0.42 mmol) and $Pr(NO_3)_3{\cdot}5H_2O$ (0.262 g, 0.63 mmol), yield: 66%. IR (KBr, cm^{-1}): 1607 (m), 1580 (m) [ν(C=C) and $\nu(C{=}N)_{py}$], 1454 (s), 1384 (s), 1329 (s), 1088 (m), 1040 (m), 817 (m), 786 (m), 739 (m) [$\nu(NO_3^-)$], 3276 (m), 3206 (m) [ν(NH)]. MS (ESI, *m/z*): 625 $[Pr(TPP)(NO_3)_2]^+$.

$[Nd(TPP)(NO_3)_2][Nd(NO_3)_3]NO_3{\cdot}6H_2O$ (Nd-TPP). TPP (0.195 g, 0.54 mmol) and $Nd(NO_3)_3{\cdot}6H_2O$ (0.355 g, 0.81 mmol), yield: 36%. IR (KBr, cm^{-1}): 1606 (m), 1580 (m) [ν(C=C) and $\nu(C{=}N)_{py}$], 1434 (s), 1384 (s), 1322 (s), 1089 (m), 1037 (m), 817 (m), 789 (m), 737 (m) [$\nu(NO_3^-)$], 3278 (m), 3214 (m) [ν(NH)]. MS (ESI, *m/z*): 628 $[Nd(TPP)(NO_3)_2]^+$. $C_{21}H_{36}N_{12}Nd_2O_{24}$ (1128.60): calcd. C 22.3, N 14.9, H 3.2; found C 25.9, N 14.2, H 2.9.

$[Sm(TPP)(NO_3)_2]NO_3{\cdot}2H_2O$ (Sm-TPP). TPP (0.195 g, 0.54 mmol) and $Sm(NO_3)_3{\cdot}6H_2O$ (0.360 g, 0.81 mmol), yield: 47%. IR (KBr, cm^{-1}): 1606 (m), 1578 (m) [ν(C=C) and $\nu(C{=}N)_{py}$], 1470 (s), 1384 (s), 1305 (s), 1082 (m), 1035 (m), 792 (m), 739 (m) [$\nu(NO_3^-)$], 3256 (m), 3199 (m) [ν(NH)]. MS (ESI, *m/z*): 634 $[Sm(TPP)(NO_3)_2]^+$.

$[Eu(TPP)(NO_3)_2]NO_3$ (Eu-TPP). TPP (0.180 g, 0.50 mmol) and $Eu(NO_3)_3{\cdot}5H_2O$ (0.321 g, 0.75 mmol), yield: 34%. IR (KBr, cm^{-1}): 1606 (m), 1578 (m) [ν(C=C) and $\nu(C{=}N)_{py}$], 1472 (s), 1384 (s), 1304 (s), 1083 (m), 1035 (m), 793 (m), 727 (w) [$\nu(NO_3^-)$], 3262 (m), 3208 (m) [ν(NH)]. MS (ESI, *m/z*): 636 $[Eu(TPP)(NO_3)_2]^+$.

$[Gd(TPP)(NO_3)_2]NO_3$ (Gd-TPP). TPP (0.184 g, 0.51 mmol) and $Gd(NO_3)_3{\cdot}6H_2O$ (0.345 g, 0.76 mmol), yield: 40% IR (KBr, cm^{-1}): 1605 (m), 1578 (m) [ν(C=C) and $\nu(C{=}N)_{py}$], 1438 (m), 1384 (s), 1323 (m), 1084 (m), 1030 (m), 813 (m), 797 (m), 735 (m) [$\nu(NO_3^-)$], 3300 (m), 3192 (m) [ν(NH)]. MS (ESI, *m/z*): 641 $[Gd(TPP)(NO_3)_2]^+$.

$[Tb(TPP)(NO_3)_2]NO_3$ (Tb-TPP). TPP (0.130 g, 0.36 mmol) and $Tb(NO_3)_3{\cdot}6H_2O$ (0.245 g, 0.54 mmol), yield: 35%. IR (KBr, cm^{-1}): 1605 (m), 1578 (m) [ν(C=C) and $\nu(C{=}N)_{py}$], 1439 (m), 1384 (s), 1321 (m), 1085 (m), 1030 (m), 797 (m), 736 (w) [$\nu(NO_3^-)$], 3300 (m), 3189 (m) [ν(NH)]. MS (ESI, *m/z*): 643 $[Tb(TPP)(NO_3)_2]^+$, 361 $[TPP + H]^+$.

$[Dy(TPP)(NO_3)_2]NO_3$ (Dy-TPP). TPP (0.173 g, 0.48 mmol) and $Dy(NO_3)_3{\cdot}5H_2O$ (0.316 g, 0.72 mmol), yield: 50%. IR (KBr, cm^{-1}): 1605 (m), 1578 (m) [ν(C=C) and $\nu(C{=}N)_{py}$], 1439 (s), 1383 (s), 1321 (s), 1085 (m), 1030 (m), 813 (m), 797 (m), 737 (m) [$\nu(NO_3^-)$], 3299 (m), 3191 (m) [ν(NH)]. MS (ESI, *m/z*): 646 $[Dy(TPP)(NO_3)_2]^+$.

dx.doi.org/10.1021/ic400389d | *Inorg. Chem.* 2013, 52, 6062−6072

Table 1. Crystal Data and Structure Refinement for the Complexes

	(La-TPP)	(Ce-TPP)	(Pr-TPP)	(Sm-TPP)	(Eu-TPP)
formula	$C_{21}H_{31.8}N_9O_{13}La$	$C_{21}H_{31.75}N_9O_{12.88}Ce$	$C_{21}H_{24}N_{10.5}O_{18.5}Pr_{1.5}$	$C_{21}H_{24}N_9O_{10}Sm$	$C_{21}H_{24}N_9O_9Eu$
mol wt	757.34	756.42	930.87	712.84	698.45
cryst syst	monoclinic	monoclinic	monoclinic	triclinic	triclinic
space group	$P2_1/c$	$P2_1/c$	$P2_1/n$	$\bar{P}1$	$\bar{P}1$
a (Å) α (deg)	19.486(2)	19.432(2)	12.433(4)	9.285(3) 93.511(4)	9.1341(18)
b (Å) β (deg)	14.7533(16) 107.949(2)	14.7193(16) 107.960(2)	18.068(5) 99.723(5)	11.016(3) 99.289(4)	76.119(3) 12.361(2)
c (Å) γ (deg)	22.087(2)	22.064(2)	15.100(5)	13.292(4) 90.546(4)	70.426(3) 12.714(3) 70.934(3)
V (Å^3)	6040.6(11)	6003.2(11)	3343.4(17)	1338.9(6)	1264.6(4)
Z	8	8	4	2	2
D(calc) (Mg/m^3)	1.666	1.674	1.849	1.768	1.834
μ (1/mm)	1.491	1.593	2.263	2.264	2.550
R_{int}	0.0616	0.0528	0.0747	0.0446	0.0262
R_1[a]	0.0550	0.0481	0.0648	0.0833	0.0325
wR_2 (all data)[b]	0.1844	0.1536	0. 1738	0.2692	0.0870
	(Gd-TPP)	(Tb-TPP)	(Dy-TPP)	(Ho-TPP)	(Er-TPP)
formula	$C_{21}H_{24}N_9O_9Gd$	$C_{21}H_{24}N_9O_9Tb$	$C_{21}H_{24}N_9O_9Dy$	$C_{21}H_{24}N_9O_9Ho$	$C_{21}H_{24}N_9O_9Er$
mol wt	703.74	705.41	708.99	711.42	713.75
cryst syst	triclinic	triclinic	triclinic	triclinic	triclinic
space group	$\bar{P}1$	$\bar{P}1$	$\bar{P}1$	$\bar{P}1$	$\bar{P}1$
a (Å) α (deg)	9.1224(9) 76.218(2)	128(3) 76.091(6)	9.1010(8) 76.2050(10)	9.100(5) 76.290(8)	9.1084(11) 76.171(2)
b (Å) β (deg)	12.3488(12) 70.388(2)	12.338(4) 70.232(6)	12.3295(11) 69.9640(10)	12.330(7) 69.967(8)	12.3171(14) 69.805(2)
c (Å) γ (deg)	12.7052(12) 70.981(2)	12.708(5) 70.823(5)	12.7126(11) 70.8610(10)	12.705(7) 70.849(8)	12.7117(15) 70.689(2)
V (Å^3)	1261.2(2)	1258.6(8)	1253.23(19)	1252.7(11)	1250.5(3)
Z	2	2	2	2	2
D(calc) (Mg/m^3)	1.853	1.861	1.879	1.886	1.896
μ (1/mm)	2.700	2.880	3.052	3.229	3.427
R_{int}	0.0280	0.0482	0.0215	0.0249	0.0240
R_1[a]	0.0339	0.0531	0.0268	0.0232	0.0305
wR_2 (all data)[b]	0.0838	0.1365	0.0707	0.0572	0.0780
	(Tm-TPP)	(Yb-TPP)	(LaT-TPP)	(GdT-TPP)	
formula	$C_{21}H_{24}N_9O_9Tm$	$C_{21}H_{24}N_9O_9Yb$	$C_{24}H_{21}N_6O_{10}S_3F_9La$	$C_{24}H_{26}N_6O_{11}S_3F_9Gd$	
mol wt	715.42	719.53	959.56	998.94	
cryst syst	triclinic	triclinic	monoclinic	triclinic	
space group	$\bar{P}1$	$\bar{P}1$	$P2_1/c$	$\bar{P}1$	
a (Å) α (deg)	9.1098(10) 76.126(2)	9.1094(9) 76.046(2)	13.7035(13)	8.5535(15) 100.506(3)	
b (Å) β (deg)	12.3241(13) 69.585(2)	12.3180(13) 69.413(2)	10.1687(9) 100.383(2)	11.910(2) 91.213(3)	
c (Å) γ (deg)	12.7311(14) 70.676(2)	12.7350(13) 70.567(2)	24.877(2)	17.815(3) 95.165(3)	
V (Å^3)	1251.5(2)	1249.0(2)	3409.8(5)	1775.8(5)	
Z	2	2	4	2	
D(calc) (Mg/m^3)	1.898	1.913	1.869	1.868	
μ (1/mm)	3.616	3.815	1.547	2.154	
R_{int}	0.0202	0.0206	0.0424	0.0331	
R_1[a]	0.0314	0.0193	0.0399	0.0409	
wR_2 (all data)[b]	0.0656	0.0485	0.1095	0.1077	

[a] $R_1 = \sum||F_o| - |F_c||/\sum|F_o|$. [b] $wR_2 = \{\sum[w(|F_o|^2 - |F_c|^2)^2]/\sum[w(F_o^4)]\}^{1/2}$.

[Ho(TPP)(NO$_3$)$_2$]NO$_3$ (Ho-TPP). TPP (0.173 g, 0.48 mmol) and $Ho(NO_3)_3{\cdot}5H_2O$ (0.317 g, 0.72 mmol), yield: 47%. IR (KBr, cm^{-1}): 1581 (m) [ν(C═C) and $\nu(C{=}N)_{py}$], 1483 (m), 1384 (m), 1325 (m), 1084 (w), 1033 (w), 814 (m) [$\nu(NO_3^-)$], 3238 (m) [ν(NH)]. MS (ESI, m/z): 649 $[Ho(TPP)(NO_3)_2]^+$.

[Er(TPP)(NO$_3$)$_2$]NO$_3$ (Er-TPP). TPP (0.130 g, 0.54 mmol) and $Er(NO_3)_3.5H_2O$ (0.239 g, 0.54 mmol), Yield: 48%. IR (KBr, cm^{-1}): 1605 (m), 1578 (m) [ν(C═C) and $\nu(C{=}N)_{py}$], 1439 (m), 1383 (s), 1322 (s), 1085 (m), 1031 (m), 797 (m) [$\nu(NO_3^-)$], 3300 (m), 3191 (m) [ν(NH)]. MS (ESI, m/z): 652 $[Er(TPP)(NO_3)_2]^+$, 361 [TPP + H]$^+$.

[Tm(TPP)(NO$_3$)$_2$]NO$_3$ (Tm-TPP). TPP (0.216 g, 0.60 mmol) and $Tm(NO_3)_3{\cdot}5H_2O$ (0.400 g, 0.90 mmol), yield: 40%. IR (KBr, cm^{-1}): 1611 (m), 1580 (m) [ν(C═C) and $\nu(C{=}N)_{py}$], 1492 (s), 1384 (s), 1302 (s), 1083 (m), 1028 (m), 812 (m), 795 (m) [$\nu(NO_3^-)$], 3271 (m), 3205 (m) [ν(NH)]. MS (ESI, m/z): 653 $[Tm(TPP)(NO_3)_2]^+$, 361 [TPP + H]$^+$.

[Yb(TPP)(NO$_3$)$_2$]NO$_3$ (Yb-TPP). TPP (0.216 g, 0.60 mmol) and $Yb(NO_3)_3{\cdot}5H_2O$ (0.404 g, 0.90 mmol), yield: 26%. IR (KBr, cm^{-1}): 1611 (m), 1580 (m) [ν(C═C) and $\nu(C{=}N)_{py}$], 1439 (s), 1384 (s), 1303 (s), 1084 (m), 1029 (m), 812 (m), 796 (m) [$\nu(NO_3^-)$], 3271 (m), 3205 (m) [ν(NH)]. MS (ESI, m/z): 658 $[Yb(TPP)(NO_3)_2]^+$, 361 [TPP + H]$^+$.

[Lu(TPP)(NO$_3$)$_2$][Lu(NO$_3$)$_3$]NO$_3$·H$_2$O (Lu-TPP). TPP (0.216 g, 0.60 mmol) and $Lu(NO_3)_3.H_2O$ (0.341 g, 0.90 mmol), yield: 30%. IR (KBr, cm^{-1}): 1610 (m), 1579 (m) [ν(C═C) and $\nu(C{=}N)_{py}$], 1452 (m), 1384 (s), 1304 (m), 1084 (m), 1038 (m), 793 (m) [$\nu(NO_3^-)$], 3268 (m) [ν(NH)]. MS (ESI, m/z): 659 $[Lu(TPP)(NO_3)_2]^+$, 361 [TPP + H]$^+$. $C_{21}H_{26}Lu_2N_{12}O_{19}$ (1100.03): calcd. C 22.9, N 15.3, H 2.4; found C 24.0, N 14.4, H 2.9.

dx.doi.org/10.1021/ic400389d | Inorg. Chem. 2013, 52, 6062−6072

Table 2. Selected Bond Lengths (Å) of the Metal Coordination Environment, Obtained from the X-ray Crystal Structures (La-TPP)−(Pr-TPP)

	(La-TPP) A	(La-TPP) B	(Ce-TPP) A	(Ce-TPP) B	(Pr-TPP)
Ln1−N(1)	2.754(7)		2.761(6)		2.702(9)
Ln1−N(2)	2.734(7)		2.699(6)		2.704(9)
Ln1−N(3)	2.748(8)		2.737(6)		2.760(8)
Ln1−N(4)	2.716(7)		2.708(6)		2.721(9)
Ln1−N(5)	2.769(8)		2.738(5)		2.725(10)
Ln1−N(6)	2.726(8)		2.712(6)		2.673(8)
Ln1−O(1)	2.570(6)		2.547(5)		2.530(8)
Ln1−O(2)	2.572(6)		2.554(5)		2.555(7)
Ln1−O(3)	2.582(6)		2.549(5)		2.513(8)
Ln1−O(1N)	2.50(3)		2.50(4)		2.55(5)
Ln1−O(2N)	2.65(3)		2.61(3)		2.52(5)
Ln2−N(7)		2.768(6)		2.755(5)	
Ln2−N(8)		2.733(8)		2.725(5)	
Ln2−N(9)		2.770(7)		2.711(6)	
Ln2−N(10)		2.727(7)		2.702(6)	
Ln2−N(11)		2.734(7)		2.750(6)	
Ln2−N(12)		2.735(7)		2.719(6)	
Ln2−O(4N)		2.54(5)		2.53(3)	
Ln2−O(5N)		2.55(4)		2.50(3)	
Ln2−O(4)		2.552(6)		2.552(5)	
Ln2−O(5)		2.571(6)		2.528(5)	
Ln2−O(6)		2.567(6)		2.544(5)	

$[La(TPP)(CF_3SO_3)_3(H_2O)]$ (LaT-TPP). TPP (0.123 g, 0.34 mmol) and $La(CF_3SO_3)_3{\cdot}H_2O$ (0.308 g, 0.51 mmol), yield: 30%. IR (KBr, cm^{-1}): 1607 (m), 1581 (m) [ν(C═C) and $\nu(C{=}N)_{py}$], 1659 (m), 1637 (m), 1298 (s), 1243 (s), 1186 (s), 1161 (m), 1030 (s) [$\nu(CF_3SO_3^-)$], 3290 (m) [ν(NH)]. MS (ESI, m/z): 797 $[La(TPP)(CF_3SO_3)_2]^+$.

$[Gd(TPP)(CF_3SO_3)(H_2O)_2](CF_3SO_3)_2$ (GdT-TPP). TPP (0.101 g, 0.28 mmol) and $Gd(CF_3SO_3)_3$ (0.254 g, 0.42 mmol), yield: 50%. IR (KBr, cm^{-1}): 1608 (m), 1581 (m) [ν(C═C) and $\nu(C{=}N)_{py}$], 1662 (m), 1640 (m), 1304 (s), 1244 (s), 1183 (s), 1146 (m), 1029 (s) [$\nu(CF_3SO_3^-)$], 3279 (m), 3239 (m) [ν(NH)]. MS (ESI, m/z): 816 $[Gd(TPP)(CF_3SO_3)_2]^+$.

Crystal Structure Determinations. Measurements were made on a BRUKER Smart-CCD-1000. Graphite monochromated Mo Kα was used. All data were corrected by Lorentz and polarization effects. Empirical absorption corrections were also applied.[21] Complex scattering factors were taken from the program package SHELX-97.[22] The structures were solved by direct methods using SIR-92[23] which revealed the position of all non-hydrogen atoms. All the structures were refined on F^2 by a full-matrix least-squares procedure using anisotropic displacement parameters for all non-hydrogen atoms. The hydrogen atoms of the carbons were located in their calculated positions and refined using a riding model. The hydrogen atoms of the amine groups were located on a difference Fourier map and refined isotropically. Molecular graphics were generated using WebLAB ViewerPro 4.0 and ORTEP-3.[24]

Computational Methods. All calculations were performed employing DFT within the hybrid meta generalized gradient approximation (hybrid meta-GGA), with the TPSSh exchange-correlation functional,[25] and the Gaussian 09 package (Revision A.02).[26] Previous studies demonstrated that the TPSSh functional provides more accurate geometries of Ln^{3+} complexes than the popular B3LYP functional,[27] as well as accurate ^{17}O A_{iso} values of the coordinated water molecule for different Gd^{3+} complexes with polyaminocarboxylate ligands.[28] Full geometry optimizations of the $[Ln(TPP)(H_2O)_q]^{3+}$ systems (Ln = La, Pr, Eu, Tb, Er or Yb, q = 3 or 4) were performed aqueous solution by using the large-core relativistic effective core potential (LCRECP) of Dolg et al. and the related [5s4p3d]-GTO valence basis set for the lanthanides,[29] and the standard 6-31G(d,p) basis set for C, H, N, and O atoms. This LCRECP includes 46 + 4f^n electrons in the core for the lanthanide, leaving the outermost 11 electrons to be treated explicitly. The use of LCRECP has been justified by the fact that 4f orbitals do not significantly contribute to bonding due to their limited radial extension as compared to the 5d and 6s shells.[30,31] LCRECP calculations were shown to provide good results in DFT studies that focus on the structure, dynamics, and estimates of relative energies of Ln^{3+} complexes.[32] No symmetry constraints have been imposed during the optimizations. The default values for the integration grid (75 radial shells and 302 angular points) and the SCF energy convergence criteria (10^{-8}) were used in all calculations. The stationary points found on the potential energy surfaces as a result of the geometry optimizations have been tested to represent energy minima rather than saddle points via frequency analysis.

The relative free energies of the different conformations of $[Ln(TPP)(H_2O)_3]^{3+}$ complexes were calculated in aqueous solution at the TPSSh/LCRECP/6-31G(d,p) level, and they include non-potential-energy contributions (zero point energies and thermal terms) obtained through frequency analysis. The enantiomerization process in $[Pr(TPP)(H_2O)_4]^{3+}$ complex was investigated by means of the synchronous transit-guided quasi-Newton method.[33] The nature of the saddle points (one imaginary frequency) was characterized by frequency analysis. The free energy barriers calculated include nonpotential energy contributions obtained by frequency analysis.

Solvent effects (water) were evaluated by using the polarizable continuum model (PCM), in which the solute cavity is built as an envelope of spheres centered on atoms or atomic groups with appropriate radii. In particular, we used the integral equation formalism (IEFPCM) variant as implemented in Gaussian 09.[34]

RESULTS AND DISCUSSION

Synthesis and Characterization of the Complexes. The Ln^{3+} complexes of TPP were obtained with 26−63% yields by direct reaction between the ligand and the appropriate hydrated lanthanide nitrate or triflate salts in methanol. The molecular formulas of all complexes was determined by the X-ray analysis except for Nd-TPP and Lu-TPP, for which elemental microanalysis was performed. The complexes were characterized by IR, ESI-MS, NMR spectroscopy, and DFT

dx.doi.org/10.1021/ic400389d | Inorg. Chem. 2013, 52, 6062−6072

Table 3. Selected Bond Lengths (Å) of the Metal Coordination Environment, Obtained from the X-ray Crystal Structures (Sm-TPP)−(Yb-TPP), (LaT-TPP), and (GdT-TPP)

	(Sm-TPP)	(Eu-TPP)	(Gd-TPP)	(Tb-TPP)	(Dy-TPP)	(Ho-TPP)	(Er-TPP)	(Tm-TPP)	(Yb-TPP)	(LaT-TPP)	(GdT-TPP)
Ln1−N(1)	2.609(11)	2.567(4)	2.532(3)	2.519(6)	2.531(3)	2.526(3)	2.521(3)	2.516(3)	2.494(2)	2.745(4)	2.590(5)
Ln1−N(2)	2.636(11)	2.597(4)	2.625(3)	2.611(7)	2.600(3)	2.560(3)	2.546(3)	2.580(3)	2.571(3)	2.737(4)	2.555(5)
Ln1−N(3)	2.599(11)	2.622(3)	2.548(4)	2.548(7)	2.520(3)	2.591(3)	2.584(3)	2.503(3)	2.502(3)	2.714(5)	2.581(5)
Ln1−N(4)	2.586(11)	2.539(4)	2.590(3)	2.575(6)	2.503(3)	2.499(3)	2.494(3)	2.478(3)	2.535(3)	2.722(5)	2.579(5)
Ln1−N(5)	2.625(10)	2.541(4)	2.615(3)	2.618(6)	2.597(3)	2.514(3)	2.500(3)	2.578(3)	2.572(2)	2.747(4)	2.541(5)
Ln1−N(6)	2.594(13)	2.620(4)	2.534(3)	2.520(6)	2.564(3)	2.593(3)	2.587(3)	2.541(3)	2.467(2)	2.746(4)	2.568(5)
Ln1−O(1N)	2.534(12)	2.550(3)	2.484(3)	2.480(6)	2.482(3)	2.466(3)	2.460(3)	2.449(3)	2.427(2)		
Ln1−O(2N)	2.591(12)	2.522(4)	2.541(3)	2.527(6)	2.509(3)	2.499(3)	2.494(3)	2.489(3)	2.481(2)		
Ln1-O(4N)	2.494(10)	2.556(4)	2.502(3)	2.525(6)	2.468(3)	2.500(3)	2.491(3)	2.438(3)	2.481(2)		
Ln1−O(5N)	2.585(10)	2.504(3)	2.534(3)	2.487(6)	2.508(3)	2.449(3)	2.438(3)	2.481(3)	2.440(2)		
Ln1−O(1)										2.557(4)	
Ln1−O(4)										2.554(4)	
Ln1−O(7)										2.570(4)	2.406(4)
Ln1−O(1w)										2.611(4)	2.411(4)
Ln1−O(2w)											2.446(4)

calculations. The IR spectra (KBr discs) show the expected shifted and splitted bands associated with ν(C═N) and ν(C═C) vibrations of the pyridine rings, suggesting interaction between the metal ions and the pyridinic nitrogen atoms.[35] Additionally, the spectra of the nitrate complexes show several bands between 1300 and 1500 cm^{-1} due to the presence of free and coordinated nitrate groups,[36] while the bands attributable to free and coordinated triflate groups appear at 1659, 1637, 1298, 1243, 1186, 1160, and 1030 cm^{-1}.[37] In some cases, bands in the range 3200−3500 cm^{-1}, corresponding to the NH groups present in the molecule, can be also observed. However, these bands are often masked by a broad signal centered at 3500 cm^{-1} due to the presence of water molecules. The mass spectra (ESI) of the compounds display the peak corresponding to the $[Ln(TPP)(NO_3)_2]^+$ fragment ($[Ln(TPP)(CF_3SO_3)_2]^+$, for (**LaT-TPP**) and (**GdT-TPP**)), which confirms the formation of all the lanthanide complexes. In some nitrate complexes a peak at m/z = 361 corresponding to $[TPP + H]^+$ is also present.

X-ray Crystal Structures. Single crystals of all compounds synthesized, except (**Nd-TPP**) and (**Lu-TPP**), were obtained by slow evaporation of an aqueous solution of the corresponding complex and used for X-ray diffraction analyses. Crystal data of all compounds are collected in Table 1, while selected bond lengths of the lanthanide coordination environments are given in Tables 2 and 3. Compounds (**La-TPP**) and (**Ce-TPP**) are isostructural, and they crystallize in the monoclinic space group $P2_1/c$. The asymmetric unit consists of two crystallographically independent half molecules of $[(Ln(TPP))_2\text{-}\mu\text{-}(NO_3)(H_2O)_6]^{5+}$ (Ln = La or Ce) (Figure 1a), five independent nitrate ions, and four uncoordinated water molecules with occupancy factors lower than one. The two half molecules present in the asymmetric unit present slightly different bond distances and angles of the metal coordination environments. Compound (**Pr-TPP**) crystallizes in the monoclinic $P2_1/n$ space group, and the asymmetric unit shows half molecule of $[(Pr(TPP))_2\text{-}\mu\text{-}(NO_3)(H_2O)_6]^{5+}$, half anionic complex $[Pr(NO_3)_6]^{3-}$, an independent nitrate ion and two water molecules of crystallization.

Compounds (**Sm-TPP**)−(**Yb-TPP**) crystallize all in the $\bar{P}1$ triclinic space group and consist of the complex $[Ln(TPP)(NO_3)_2]^+$ and an independent nitrate ion. (**Sm-TPP**) also shows two water molecules of solvation. (**LaT-TPP**) crystallizes, as (**La-TPP**) and (**Ce-TPP**), in the monoclinic space group $P2_1/c$, and only the monomeric neutral complex $[La(TPP)(CF_3SO_3)_3(H_2O)]$ is present in the asymmetric unit. (**GdT-TPP**) crystallizes in the $\bar{P}1$ triclinic group and contains the cation $[Gd(TPP)(CF_3SO_3)(H_2O)_2]^{+2}$ and two independent triflate ions.

The dimeric molecules $[(Ln(TPP))_2\text{-}\mu\text{-}(NO_3)(H_2O)_6]^{5+}$ (Ln = La, Ce or Pr) present in (**La-TPP**), (**Ce-TPP**), and (**Pr-TPP**) are very similar. Each cationic dimer is comprised by two $[Ln(TPP)(H_2O)_3]^{3+}$ unities joined by a disordered nitrate group. In these $[Ln(TPP)(H_2O)_3]^{3+}$ cationic species, the metal ion is placed into the macrocyclic cavity coordinated by the six nitrogen atoms of the ligand. Ten coordination is completed by three oxygen atoms of three coordinated water molecules located on one side of the plane defined by the macrocyclic ligand, and an oxygen atom of the bridging nitrate group placed on the opposite side (Figure 1a). The nitrogen atom of the bridging nitrate group is located in an inversion center that relates the two $[Ln(TPP)(H_2O)_3]^{3+}$ subunits, and it is disordered into two positions with 50% occupancy factors. The two $[Ln(TPP)(H_2O)_3]^{3+}$ units are encapsulating the nitrate group acting as a bridge between the two metal centers, conferring a ball shape to the cationic dimer $[(Ln(TPP))_2\text{-}\mu\text{-}(NO_3)(H_2O)_6]^{5+}$ (Figure 2).

In the nitrate salts (**Sm-TPP**)−(**Yb-TPP**) the Ln^{3+} ion shows a ten-coordinate environment with the metal being bound to the six nitrogen atoms of the ligand and two bidentate nitrate groups located on opposite sides of the best plane defined by the N atoms of the ligand. (**LaT-TPP**) shows a ten coordination environment provided by the six amine nitrogen atoms from the ligand, one water molecule, and the three monodentated triflate groups. One triflate group is located at one side of the plane defined by the macrocyclic ligand, while the two remaining triflate groups and the water molecule are sited at the other side of the plane. However, in (**GdT-TPP**), the metal ion is nine coordinated through the six N atom from the ligand, two water molecules and a triflate ion, and two triflate ions remain uncoordinated.

The conformation of the TPP ligand in the complexes is not planar, and it varies along the lanthanide series. In (**La-TPP**)−(**Pr-TPP**) and (**LaT-TPP**), the pyridine units are tilted showing similar dihedral angles between the three rings of the molecule (ranging between 52 and 66°). Two groups of

dx.doi.org/10.1021/ic400389d | Inorg. Chem. 2013, 52, 6062−6072

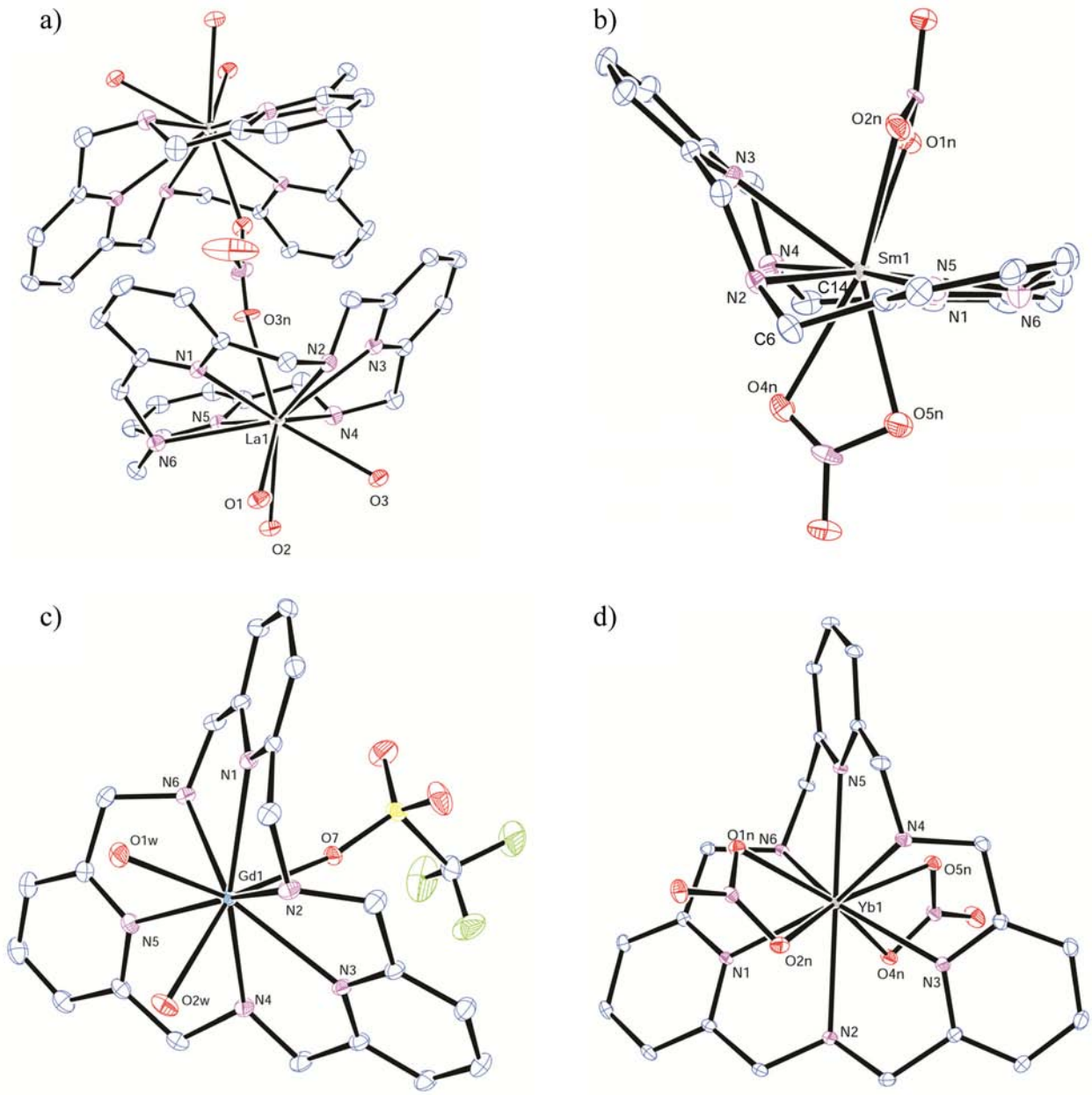

Figure 1. X-ray crystal structures of (a) $[(La(TPP))_2\text{-}\mu\text{-}(NO_3)(H_2O)_6]^{5+}$ (**La-TPP**), (b) $[Sm(TPP)(NO_3)_2]^+$ (**Sm-TPP**), (c) $[Gd(TPP)(CF_3SO_3)(H_2O)_2]^{2+}$ (**GdT-TPP**), and (d) $[Yb(TPP)(NO_3)_2]^+$ (**Yb-TPP**) showing the atomic numbering scheme. Hydrogen atoms are omitted for simplicity. The ORTEP plots are at the 10% probability level.

torsion angles N_{py}–C–C–N_{am} (with values of ca 43° and 24°) were found alternatively distributed in the molecule. All the torsion angles show the same sign, so that the TPP ligand in each monomer is shaped like a truncated cone, while the symmetry approaches C_3. All the NH groups are pointing toward the smaller base of the truncated cone in a *syn* conformation. The six macrocyclic nitrogen donors are sited on a slightly distorted plane with a rms deviation from planarity of 0.3371 and 0.3554 Å for (**La-TPP**), 0.3413 and 0.3542 Å for (**Ce-TPP**), 0.3467 Å for (**Pr-TPP**), and 0.3521 Å for (**LaT-TPP**).

In (**Eu-TPP**)–(**Yb-TPP**), the ligand is twisted; one of the N_{py}–Ln^{3+}–N_{am} angles in the molecule, (involving one of the pyridyl N atoms and the amine N atom opposite to that ring, see angle N5–Yb1–N2 for (**Yb-TPP**) in Figure 1d) takes a value near 180° [from 179.4(1)° for (**Ho-TPP**) and (**Er-TPP**) to 179.7(2)° for (**Tbh-TPP**)], while the two nearly symmetrical halves of the macrocycle are twisted around this axis. A measure of the twist angle is given by the dihedral angles defined by the pyridyl ring containing the main axis and the remaining pyridyl rings. These values take similar values for all complexes (ca 63° for one of the rings and ca 47° for the second one). As a result of their twisted structure, the symmetry of the $[Ln(TPP)(NO_3)_2]^+$ complexes in the solid state approaches C_2. Two of the NH groups are pointing to one side of the macrocycle, while the third one is pointing to the opposite side, resulting in an *anti* conformation.

The conformation of the ligand in (**Sm-TPP**) is different from that found in compounds (**Eu-TPP**)–(**Yb-TPP**). In (**Sm-TPP**), the dihedral angle between the two pyridine rings

dx.doi.org/10.1021/ic400389d | *Inorg. Chem.* 2013, 52, 6062–6072

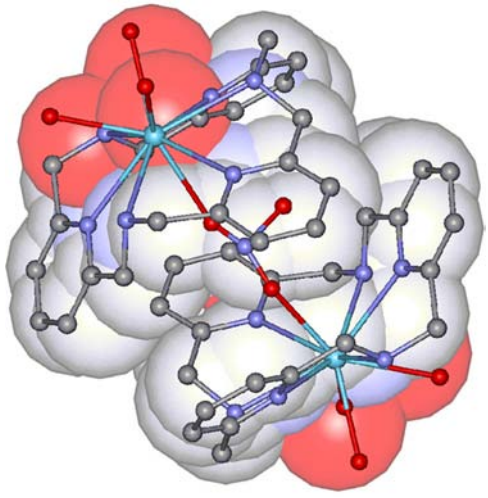

Figure 2. View of the $[(Ln(TPP))_2\text{-}\mu\text{-}(NO_3)(H_2O)_6]^{5+}$ dimer present in (**La-TPP**), (**Ce-TPP**), and (**Pr-TPP**) with the encapsulated bridging nitrate group and a ball shape.

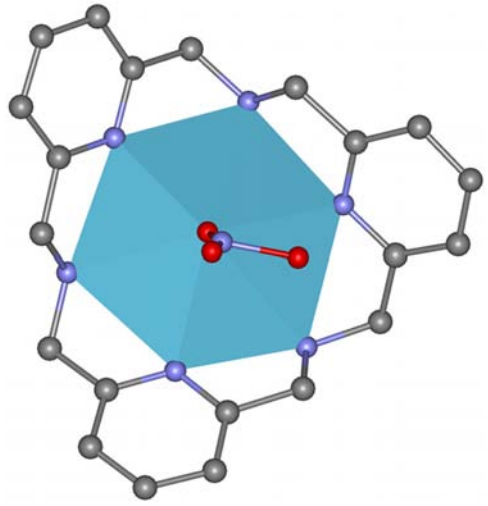

Figure 3. Hexagonal bipyramidal coordination geometry around the Ln^{3+} ion in (**La-TPP**), (**Ce-TPP**), and (**Pr-TPP**).

containing N1, C1−C5 and N5, C15−C19 is 12.8(8)°, while the dihedral angles between these rings and the remaining pyridyl unit (containing N3 and C8−C12) are bigger and quite similar [55.8(5)° and 43.6(6)°, respectively]. This disposition shows that the ligand is folded by an imaginary line connecting two methylene groups (C6 and C14, Figure 1b), which gives rise to a half chair conformation. Due to this folding conformation, the N(3)−Sm(1)−N(6) angle [150.5(5)°] is shorter than the remaining angles defined by two nitrogen atoms in opposite sides of the macrocycle, [N(1)−Sm(1)−N(4) and N(2)−Sm(1)−N(5), with values of 169.9(4) and 164.3(3)° respectively]. The two torsion angles N_{py}−C−C−N_{am} involving the pyridine ring containing N3 are negative, and the amine protons bound to N2 and N4 groups are directed toward the outside of the bend while the N(6)−H group is pointing inward. The solid state symmetry of (**5**) approaches C_s. In (**GdT-TPP**), the ligand is slightly folded as in (**Sm-TPP**) by an imaginary line connecting the amine groups [N(2) and N(6)], but the two pyridine rings [N(3), C(8)−C(12) and N(5), C(15)−C(19)] sited in one of the halves are twisted around the N(6)−Gd(1)−N(2) axis as in (**Eu-TPP**)−(**Yb-TPP**) (Figure 1d).

The Ln−N_{py} and Ln−N_{am} bond distances are similar to those previously reported for Ln^{3+} complexes containing pyridyl units.[38] An overview of all the crystal structures clearly illustrates that Ln−N and Ln−O distances decrease regularly from La^{3+} to Yb^{3+} in agreement with the lanthanide contraction[39] (see Table 2). The distances between the Ln^{3+} ion and the oxygen atoms from the nitrate groups or water molecules are shorter than those between the metal ion and the nitrogen atoms from the ligand, while in general the Ln−N_{am} bond distances are slightly shorter than the Ln−N_{py} ones.

Due to the inherent rigidity of three pyridine rings in the 18-membered macrocyclic ligand, it is not easy to assign the coordination geometry around the Ln^{3+} ion for the complexes to a regular polyhedron. However, it can be considered as a hexagonal bipyramid where, in all cases, the six nitrogen atoms from the macrocycle define the hexagonal plane (Figure 3). The position of the 6-fold axis depends on the coordination sphere of the particular complex. In (**La-TPP**)−(**Pr-TPP**) it is defined by the oxygen atom of the bridging nitrate group and, in the opposite side of the plane, by the three water molecules coordinated to the metal ion. In (**Sm-TPP**)−(**Yb-TPP**) it is be defined by the bidentate nitrate groups placed on opposite sides of the macrocycle. Finally, in (**LaT-TPP**) and (**GdT-TPP**), the 6-fold axis is defined by the coordinated triflate and water molecules.

Analysis of the short inter- and intramolecular ring−ring interactions reveals the presence of face-to-face π,π-stacking interactions between the pyridyl groups of adjacent dimers in (**La-TPP**). The dihedral angle between the planes containing the pyridyl rings is 19.56°, while the distances between the centroids are 4.16 Å.[40] Hydrogen bond interactions involving the hydrogen atoms of the secondary amine nitrogen groups from the ligand and the nitrate and triflate anions are present in the solid state structures of all compounds (Table S2, Supporting Information). Similar hydrogen bond interactions have been previously reported for other lanthanide complexes.[38]

Structure in Solution of the Complexes with the Lightest Ln^{3+} ions (Ln = La−Sm). The ^{1}H NMR spectrum of the diamagnetic $[La(TPP)]^{3+}$ complex recorded in D_2O solution at pH 6.0 shows five resonances (Figure 4, see also Table 4): one signal at 3.87 ppm attributable to the NH protons of the ligand, two signals due to the proton nuclei of

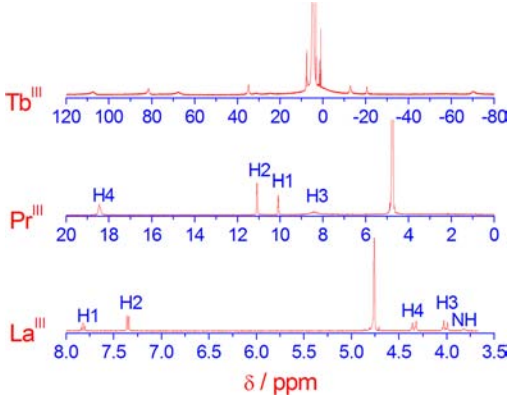

Figure 4. ^{1}H NMR spectra of $[Ln(TPP)]^{3+}$ complexes recorded in D_2O solution at 298 K and pH 6.0 (400 MHz).

dx.doi.org/10.1021/ic400389d | Inorg. Chem. 2013, 52, 6062−6072

Table 4. ^{1}H NMR Shifts (ppm) Observed for Ln^{3+} Complexes of TPP in D_2O Solution at 298 K and pH 6.0

	La	Ce	Pr	Nd	Sm[a]
H1	7.88	8.87	10.15	9.53	8.03
H2	7.41	8.87	11.14	10.15	7.67
H3	4.07	5.43	8.05	8.9	4.06
H4	4.40	10.07	18.48	14.32	5.46

[a]Only the chemical shifts corresponding to the major species observed in solution are reported.

the pyridyl units, and two signals due to the methylenic protons, which give an AB spin system with ^2J = 15 Hz. This points to an effective C_{3v} symmetry of the complex in solution confirmed by the ^{13}C NMR spectrum, which shows 4 signals for the 21 carbon nuclei of the ligand backbone (δ = 54.2, 122.2, 139.9, and 158.1 ppm). A similar situation is observed in the ^{1}H NMR spectra of the paramagnetic Ce^{3+}, Pr^{3+}, and Nd^{3+} ions (Figure 4), which present four signals (excluding those of the NH protons) and thus are in agreement with an effective C_{3v} symmetry of the complexes in solution. The situation changes for the Sm^{3+} complex, for which the ^{1}H NMR spectrum evidence the presence of two species in solution: a major complex species with an effective C_{3v} symmetry and a second less abundant species with a lower symmetry, with relative populations of 60:40.

Assuming that these complexes adopt a similar structure in the solid state and in solution, one would expect a C_3 symmetry, which should provide eight proton signals including one due to the ligand NH groups. Most likely dynamic intramolecular exchange processes result in an effective C_{3v} symmetry averaging the two proton signals expected for H2 within the C_3 point group. For a C_3 symmetry, the methylenic protons of the ligand should give four signals, two corresponding to the CH_2 protons pointing to the smaller base of the truncated cone and another two for the CH_2 protons pointing in the opposite direction. The presence of two signals, with an AB spin pattern in the case of the La^{3+} complex, exclude however a dynamic exchange process involving complex dissociation.

The ^{1}H NMR spectra of solutions of compounds (**La-TPP**) and (**LaT-TPP**) in D_2O are virtually identical, indicating that the nitrate ligand observed in the solid state for compounds (**La-TPP**)−(**Pr-TPP**), and the triflate ligands found in (**LaT-TPP**), are replaced by water molecules upon dissolution of the complexes in water.[41] Thus, to obtain information on the solution structure and dynamics complexes of TPP with the lightest Ln^{3+} ions, we have characterized the $[Ln(TPP)(H_2O)_4]^{3+}$ systems (Ln = La or Pr) by means of DFT calculations (TPSSh model, see Figure 5). Geometry optimizations provided a minimum energy conformation that resembles the corresponding X-ray crystal structures, where ligand adopts a *syn* conformation. The bond distances between the lanthanoid and the coordinating donor atoms of the ligand are in very good agreement with the ones found in the crystal structures (see Supporting Information) with average unsigned deviations of only 1.1 and 1.0% for the complexes of La^{3+} and Pr^{3+}, respectively.

For a given nucleus *i*, the isotropic paramagnetic shift induced by a lanthanide ion *j* (δ_{ij}^{para}) is generally a combination of the Fermi contact (δ_{ij}^{con}) and dipolar (δ_{ij}^{dip}) contributions:[42]

$$\delta_{ij}^{para} = \delta_{ij}^{exp} - \delta_i^{dia} = \delta_{ij}^{con} + \delta_{ij}^{dip} \quad (1)$$

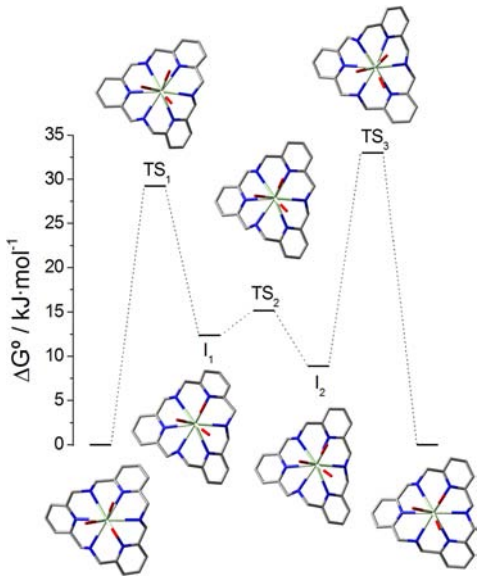

Figure 5. Relative free energies of minima, intermediates (I), and transition states (TS) obtained from DFT calculations for the enantiomerization process of $[Pr(TPP)(H_2O)_4]^{3+}$.

where δ_{ij}^{exp} represents the experimentally observed chemical shift and δ_i^{dia} denotes the diamagnetic contribution, which can be estimated by measuring the chemical shifts for analogous diamagnetic complexes (La^{3+}, Lu^{3+}, or Y^{3+}). In the present case, the ^{1}H NMR shifts observed for the La^{3+} complex were used to estimate the diamagnetic contribution. Contact shifts arise from through-bond transmission of unpaired electron-spin density from the Ln^{3+} ion to the nucleus under study, and they can be expressed as in eq 2:

$$\delta_{ij}^{con} = \langle S_z \rangle_j \frac{\mu_B}{3kT\gamma_I} \frac{A}{\hbar} 10^6 = \langle S_z \rangle_j F_i \quad (2)$$

where $\langle S_z \rangle$ is the reduced value of the average spin polarization, μ_B is the Bohr magneton, k the Boltzmann constant, γ_I the gyromagnetic ratio of the observed nucleus, $A/\hbar$ is the hyperfine coupling constant (HFCC, rad/s), and δ_{ij}^{con} is expressed in parts per million. The pseudocontact contribution results from the local magnetic field induced in the nucleus under study by the magnetic moment of the Ln^{3+} ion and, for a system with axial symmetry, can be written as in eq 3:

$$\delta_{ij}^{dip} = \frac{C_j {\mu_B}^2}{60k^2T^2}\left[\frac{A_2^0\langle r^2\rangle(3\cos^2\theta - 1)}{r^3}\right] \quad (3)$$

Here C_j is the Bleaney's constant,[43] characteristic of the Ln^{3+} ion, and $A_2^0\langle r^2\rangle$ is the ligand field coefficient of the second degree. If the principal magnetic axis system is used as the coordinate system, combination of eqs 2 and 3 gives

$$\delta_{ij}^{para} = \langle S_Z \rangle_j F_i + C_j G_i \quad (4)$$

Where G_i is proportional to the $(3\cos^2\theta - 1)/r^3$ term in eq 3. Equation 4 can be rewritten in the linear form given by eq 5:

$$\frac{\delta_{ij}^{para}}{C_j} = \frac{\langle S_Z \rangle_j}{C_j} F_i + G_i \quad (5)$$

Since $\langle S_z \rangle$ and C_j are characteristic of the Ln^{3+} ion but independent of the ligand, whereas F_i and G_i are characteristic of the nucleus under study, but independent of the Ln^{3+} ion,

dx.doi.org/10.1021/ic400389d | Inorg. Chem. 2013, 52, 6062−6072

plots according to eq 5 for a series of isostructural complexes should exhibit linear trends provided the crystal field coefficients are invariant.

The ^{1}H paramagnetic shifts observed for the Ce^{3+}, Pr^{3+}, and Nd^{3+} complexes of TPP plotted according to eq 5 give straight lines (Figure 6, $R^2 > 0.991$), which allowed a separation of the

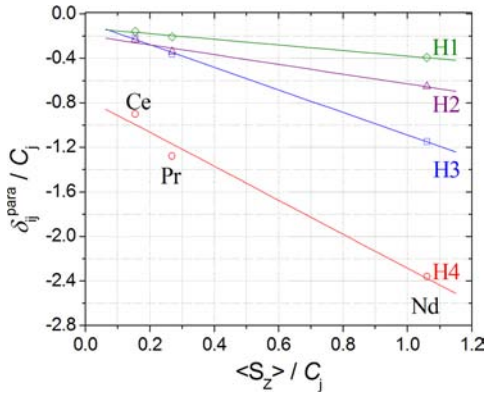

Figure 6. Plot of the paramagnetic shifts observed for Ln^{3+} complexes of TPP (Ln = Ce, Pr, and Nd) according to eq 5.

contact and pseudocontact contributions to the paramagnetic shifts. The slopes of the straight lines shown in Figure 6 provided the F_i values listed in Table 5. The contact contribution to the different paramagnetic shifts observed for the Pr^{3+} complex were obtained with eq 2 with $\langle S_z \rangle = -2.956$, which allowed us to estimate the pseudocontact contribution as well with the use of eq 1. The results show that both contact and pseudocontact mechanisms provide sizable contributions to the observed paramagnetic shifts. A plot of the pseudocontact shifts obtained by this procedure for the Pr^{3+} complex versus the geometrical factors $(3\cos^2\theta - 1)/r^3$ obtained from the DFT structure of $[Pr(TPP)(H_2O)_4]^{3+}$ gives a straight line ($R^2 > 0.996$), which indicates that our DFT calculations provide good models for the structure in solution of these complexes.

The nonplanar conformation of the TPP ligand induces chirality in $[Ln(TPP)(H_2O)_4]^{3+}$ complexes. These complexes are characterized by three $C-CH_2-NH-CH_2$ dihedral angles of ca. 177°, and another three of ca. 82°. The interconversion between the two enantiomeric forms of $[Ln(TPP)(H_2O)_4]^{3+}$ requires the inversion of these $C-CH_2-NH-CH_2$ dihedral angles of the ligand, thereby resulting on an averaged C_{3v} symmetry. Thus, the effective C_{3v} symmetry observed in the ^{1}H NMR spectra of these complexes can be attributed to a fast enantiomerization on the NMR time scale. DFT calculations performed on the $[Pr(TPP)(H_2O)_4]^{3+}$ system provide further insight into the mechanism and activation barriers involved in the dynamic process. According to our calculations, the enantiomerization process is a three step process each of them involving the modification of the two $C-CH_2-NH-CH_2$ dihedral angles affecting one of the NH groups of the ligand (Figure 5). These results are in line with different computational studies on Ln^{3+} complexes with cyclen-based ligands, which showed that the inversion of the macrocyclic ring is a four-step process each involving the inversion of a five-membered chelate ring formed upon coordination of the ethylenediamine moieties.[44] Because of the multistage nature of the ring-inversion process, the experimentally measured activation energy would be effective over the three stages shown in Figure 5. The TS endowed with the highest free energy corresponds to TS_3, whose energy amounts to 33.0 kJ/mol. This activation free energy is considerably lower than those obtained both theoretically and experimentally for the ring inversion process in cyclen-based Ln^{3+} complexes (56−65 kJ/mol).[45,46] Thus, the effective C_{3v} symmetry observed for the $[Ln(TPP)(H_2O)_4]^{3+}$ complexes in solution (Ln = La−Sm) appears to be related to a fast enantiomerization process involving the inversion of the TPP ligand.

Structure in Solution of the Complexes with the Heaviest Ln^{3+} Ions (Ln = Eu−Lu). The ^{1}H NMR spectra of the paramagnetic complexes of heavier Ln^{3+} ions recorded in D_2O at pH 6.0 show a single set of highly paramagnetically shifted resonances consisting of 10−11 signals (Figure 4). Assuming that the signals due to NH protons are not observed due to their excessive line-broadening related to their proximity to the paramagnetic center, the number of signals observed for these complexes would be in agreement with effective C_s or C_2 symmetries in solution. As pointed out above, the X-ray structure of $[Sm(TPP)(NO_3)_2]^+$ described above approaches the C_s point group, while the structures of this cation in compounds (**Eu-TPP**)−(**Yb-TPP**) is closer to the C_2 point group. A closer inspection of the latter complexes shows that an averaged C_2 symmetry required the inversion of one of the NH groups of the ligand, which was found to be very slow in different metal complexes of macrocyclic polyamines.[47]

For the smallest Ln^{3+} ions such as Er^{3+} and Yb^{3+}, geometry optimizations (TPSSh/LCRECP/6-31G(d,p) level) were initially performed on the $[Ln(TPP)(H_2O)_4]^{3+}$ systems by using the X-ray structure as input structure, and replacing the coordinated oxygen atoms of nitrate ligands by water molecules. These calculations provided nine-coordinate optimized geometries, one of the water molecules systematically leaving the metal ion coordination environment during the structure optimization process. Subsequent calculations per-

Table 5. Ln^{3+}-Induced ^{1}H NMR Paramagnetic Shifts, Contact, and Pseudocontact (Dipolar) Contributions (ppm) and Calculated Geometrical Factors for Ln^{3+} complexes of TPP at 298 K

	δ_i^{para} [a]			F_i [b]	δ_i^{con}	δ_i^{dip}	$(3\cos^2\theta - 1)/r^3$ [c]
proton	Ce	Pr	Nd	(Ce → Nd)	Pr	Pr	Pr
H1	0.99	2.27	1.65	−0.25(2)	0.74	1.53	−1.713
H2	1.46	3.73	2.74	−0.44(6)	1.30	2.43	−2.826
H3	1.36	3.98	4.83	−1.02(3)	3.01	0.97	−0.321
H4	5.67	14.08	9.92	−1.52(21)	4.50	9.58	−8.271

[a]Diamagnetic contribution estimated by using the shifts observed for the La^{3+} complex. [b]Obtained from the linear fits of the data according to eq 5. [c]Geometric factors obtained from the structure of $[Pr(TPP)(H_2O)_4]^{3+}$ optimized in aqueous solution at the TPSSh/LCRECP/6-31G(d,p) level (× 10^3 Å^{-3}). Values for symmetry equivalent nuclei have been averaged.

dx.doi.org/10.1021/ic400389d | Inorg. Chem. 2013, 52, 6062−6072

formed on the $[Er(TPP)(H_2O)_3]^{3+}$ system gave an optimized geometry in very good agreement with the solid state structure in terms of distances between the metal ion and the donor atoms of the ligand (average unsigned deviation of only 1.8%).

Full geometry optimizations of the $[Ln(TPP)(H_2O)_3]^{3+}$ systems (Ln = Eu, Tb, Er, or Yb) were performed by using as input geometries the crystal structures of compounds (**Sm-TPP**) and (**Er-TPP**), in which the two coordinated nitrate ligands were replaced by three water molecules. The relative energies of the two energy minima obtained, which have been labeled as pseudo-C_s and psudo-C_2, are shown in Figure 7. Our

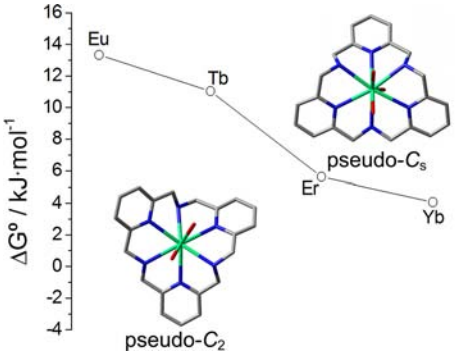

Figure 7. Relative free energies of the pseudo-C_2 and pseudo-C_s forms of $[Ln(TPP)(H_2O)_3]^{3+}$ complexes obtained at the TPSSh/LCRECP/6-31G(d,p) level. Positive energies indicate that the pseudo-C_s isomer is more stable than the pseudo-C_2 one. The geometries of the two isomers optimized for the Er^{3+} complex are shown.

calculations predict that the pseudo-C_s form is more stable than the pseudo-C_2 one by 13.3 kJ/mol in the case of the Eu^{3+} complex, a value that is reduced along the lanthanide series reaching 4.1 kJ/mol for the Yb^{3+} analogue. Thus, our calculations indicate that the $[Ln(TPP)(NO_3)_2]^+$ complexes (Ln = Eu–Lu) adopt a pseudo-C_s conformation in solution, which is compatible with the number of signals observed in the ^{1}H NMR spectra. Unfortunately, the complexity of the ^{1}H NMR spectra of these complexes did not allow confirming this by analyzing the Yb^{3+}-induced paramagnetic shifts.

The proton spectrum of the diamagnetic $[Lu(TPP)]^{3+}$ complex could not be fully assigned due to its complexity. Two groups of multiplets appear in the aromatic region due to the para and meta pyridine proton nuclei, while several doublet signals appear between 3.9 and 4.6 ppm due to the six methylenic groups. Furthermore, 12 signals appear in the ^{13}C NMR spectrum. Thus, most likely the $[Lu(TPP)]^{3+}$ complex adopts a pseudo-C_2 geometry in solution, which is stabilized as the ionic radius of the lanthanide decreases along the series (Figure 7).

CONCLUSIONS

The lanthanide complexes of the triazapyridinophane macrocycle TPP where synthesized and their structure investigated both in the solid state and in D_2O solution. The solid state structural characterization shows the presence of dimeric entities $[(Ln(TPP))_2$-μ-$(NO_3)(H_2O)_6]^{5+}$ for Ln = La, Ce, or Pr (**La-TPP**)–(**Pr-TPP**), where the TPP ligand in each monomer adopts a truncated cone conformation with a C_3 symmetry, while the solid state symmetry of the Sm^{3+} complex (**5**) approaches C_s symmetry in the solid state. The effective C_{3v} symmetry observed for (**1**)–(**5**) in solution appears to be related to a fast enantiomerization process involving the inversion of the TPP ligand. DFT calculations performed on the $[Pr(TPP)(H_2O)_4]^{3+}$ system shows that the enantiomerization process is a three step process with an activation free energy of only 33.0 kJ/mol. The ligand is twisted in the complexes of the heaviest lanthanide ions (Eu^{3+}–Yb^{3+}, (**Eu-TPP**)–(**Yb-TPP**)), to give pseudo-C_2 symmetry. However, our DFT calculations indicate that the $[Ln(TPP)(NO_3)_2]^+$ complexes (Ln = Eu–Yb) adopt a pseudo-C_s conformation in solution, which is compatible with the 10–11 paramagnetically shifted resonances observed in their ^{1}H NMR spectra.

The Ln^{3+} complexes of TPP appear to be relatively stable in aqueous solution, as dissociation of the complexes was not observed in solutions of the complexes in D_2O at pH 6 stored for several weeks. Thus, the preparation of stable Ln^{3+} complexes based on the TPP platform functionalized with different pendant arms may be envisaged.

ASSOCIATED CONTENT

Supporting Information

Comparison between experimental and calculated (DFT) bond distances, hydrogen-bonding data, and optimized Cartesian coordinates obtained with DFT calculations. This material is available free of charge via the Internet at http://pubs.acs.org.

AUTHOR INFORMATION

Corresponding Author

*E-mail address: paulo@uvigo.es.

Notes

The authors declare no competing financial interest.

ACKNOWLEDGMENTS

We thank Ministerio de Ciencia e Innovación, Plan Nacional de I+D+i (CTQ2011-24487), and Xunta de Galicia (PXIB209028PR) for financial support. The authors are indebted to Centro de Supercomputación of Galicia (CESGA) for providing the computer facilities.

REFERENCES

(1) Fricker, S. P. *Chem. Soc. Rev.* **2006**, *35*, 524–533.
(2) Jakupec, M. A.; Unfried, P.; Keppler, B. K. *Rev. Physiol. Biochem. Pharmacol.* **2005**, *153*, 101–111.
(3) Shin, B. C.; Park, K. B.; Jang, B. S.; Lim, S. M.; Shim, C. K. *Nucl. Med. Biol.* **2001**, *28* (6), 719–725.
(4) Swainston, H. T.; Scott, L. J. *Drugs* **2005**, *64*, 985–996.
(5) Roesch, F. *Radiochim. Acta* **2007**, *95*, 303–311.
(6) Hussain, A.; Gadadhar, S.; Goswami, T. K.; Karande, A. A.; Chakravarty, A. R. *Eur. J. Med. Chem.* **2012**, *50*, 319–331.
(7) (a) Merbach, A. E.; Tóth, E. *The Chemistry of Contrast Agents in Medical Magnetic Resonance Imaging*; Wiley: New York, 2001. (b) Chan, K. W. Y.; Wong, W. T. *Coord. Chem. Rev.* **2007**, *251*, 2428–2451. (c) Terreno, E.; Castelli, D. D.; Viale, A.; Aime, S. *Chem. Rev.* **2010**, *110*, 3019–3042.
(8) Bünzli, J-C. G. *Chem. Rev.* **2010**, *110*, 2729–2755.
(9) Aime, S.; Geninatti Crich, S.; Gianolino, E.; Giovenzana, G. B.; Tei, L.; Terreno, E. *Coord. Chem. Rev.* **2006**, *250*, 1562–1579.
(10) Evans, C. H. *Trends Biochem. Sci.* **1983**, 445–449.
(11) Caravan, P.; Jeffrey, J. E.; McMurry, T. J.; Lauffer, R. B. *Chem. Rev.* **1999**, *99*, 2293–2352.
(12) Mewis, R. E.; Archibald, S. J. *Coord. Chem. Rev.* **2010**, *254*, 1686–1712.
(13) (a) Sessler, J. L.; Mody, T. D.; Hemmi, G. W.; Lynch, V. *Inorg. Chem.* **1993**, *32*, 3175–3187. (b) Sessler, J. L.; Hemmi, G.; Mody, T. D.; Murai, T.; Burrell, A.; Young, S. W. *Acc. Chem. Res.* **1994**, *27*, 43–50.

(14) Young, S. W. Y.; Qing, F.; Harriman, A.; Sessler, J. L.; Dow, W. C.; Mody, T. D.; Hemmi, G. W.; Haoii, Y.; A. Miller, R. A. *Proc. Natl. Acad. Sci.* **1996**, *93*, 6610−6615.
(15) (a) Mato-Iglesias, M.; Roca-Sabio, A.; Pálinkás, Z.; Platas-Iglesias, C.; Tóth, E.; Esteban, D.; de Blas, A.; Rodríguez-Blas, T. *Inorg. Chem.* **2008**, *47*, 7840−7851. (b) Roca-Sabio, A.; Mato-Iglesias, M.; Esteban-Gómez, D.; Tóth, E.; de Blas, A.; Platas-Iglesias, C.; Rodríguez-Blas, T. *J. Am. Chem. Soc.* **2009**, *131*, 3331−3341. (c) Pálinkás, Z.; Roca-Sabio, A.; Mato-Iglesias, M.; Esteban-Gómez, D.; Platas-Iglesias, C.; de Blas, A.; Rodríguez-Blas, T.; Tóth, E. *Inorg. Chem.* **2009**, *48*, 8878−8889. (d) Roca-Sabio, A.; Mato-Iglesias, M.; Esteban-Gómez, D.; de Blas, A.; Rodríguez-Blas, T.; Platas-Iglesias, C. *Dalton Trans.* **2011**, *40*, 384−392.
(16) Bottino, F.; Di Grazia, M.; Finocchiaro, P.; Fronczek, F. R.; Mamo, A.; Pappalardo, S. *J. Org. Chem.* **1988**, *53*, 3521−3529.
(17) Lee, G.; Oka, M.; Takemura, H.; Miyahara, Y.; Shimizu, N.; Inazu, T. *J. Org. Chem.* **1996**, *61*, 8304−8306.
(18) (a) Raffard, N.; Carina, R.; Simaan, A. J.; Sainton, J.; Riviére, E.; Tchertanov, L.; Bourcier, S.; Bouchoux, G.; Delroisse, M.; Banse, F.; Girerd, J.-J. *Eur. J. Inorg. Chem.* **2001**, *51*, 2249−2254. (b) Koch, W. O.; Kaiser, J. T.; Kruger, H.-J. *Chem. Commun.* **1997**, 2237−2238. (c) Koch, W. O.; Barbieri, A.; Grodzicki, M.; Schunemann, V.; Trautwein, A. X.; Kruger, H.-J. *Angew. Chem., Int. Ed. Engl.* **1996**, *35*, 422−424.
(19) Roca-Sabio, A.; Bonnet, C. S.; Mato-Iglesias, M.; Esteban-Gómez, D.; Tóth, E.; de Blas, A.; Rodríguez-Blas, T.; Platas-Iglesias, C. *Inorg. Chem.* **2012**, *51*, 10893−10903.
(20) Viswanathan, S.; Kovacs, Z.; Green, N.; Ratnakar, S. J.; Sherry, A. D. *Chem. Rev.* **2010**, *110*, 2960−3018.
(21) Sheldrick, G. M. *SADABS. Program for Empirical Absoption Correction of Area Detector Data*; University of Götingen, Germany, 1996.
(22) Sheldrick, G. M. *SHELX-97, An integrated system for solving and refining crystal structures from diffraction data*; University of Göttingen, Germany, 1997.
(23) Altornare, A.; Cascarano, G.; Giacovazzo, C.; Gualardi, A. *J. Appl. Crystallogr.* **1993**, *26*, 343−350.
(24) ORTEP-3: Farrugia, L. J. *J. Appl. Crystallogr.* **1997**, *30*, 565.
(25) Tao, J. M.; Perdew, J. P.; Staroverov, V. N.; Scuseria, G. E. *Phys. Rev. Lett.* **2003**, *91*, 146401.
(26) Frisch, M. J.; Trucks, G. W.; Schlegel, H. B.; Scuseria, G. E.; Robb, M. A.; Cheeseman, J. R.; Scalmani, G.; Barone, V.; Mennucci, B.; Petersson, G. A.; Nakatsuji, H.; Caricato, M.; Li, X.; Hratchian, H. P.; Izmaylov, A. F.; Bloino, J.; Zheng, G.; Sonnenberg, J. L.; Hada, M.; Ehara, M.; Toyota, K.; Fukuda, R.; Hasegawa, J.; Ishida, M.; Nakajima, T.; Honda, Y.; Kitao, O.; Nakai, H.; Vreven, T.; Montgomery, J. A., Jr.; Peralta, J. E.; Ogliaro, F.; Bearpark, M.; Heyd, J. J.; Brothers, E.; Kudin, K. N.; Staroverov, V. N.; Kobayashi, R.; Normand, J.; Raghavachari, K.; Rendell, A.; Burant, J. C.; Iyengar, S. S.; Tomasi, J.; Cossi, M.; Rega, N.; Millam, N. J.; Klene, M.; Knox, J. E.; Cross, J. B.; Bakken, V.; Adamo, C.; Jaramillo, J.; Gomperts, R.; Stratmann, R. E.; Yazyev, O.; Austin, A. J.; Cammi, R.; Pomelli, C.; Ochterski, J. W.; Martin, R. L.; Morokuma, K.; Zakrzewski, V. G.; Voth, G. A.; Salvador, P.; Dannenberg, J. J.; Dapprich, S.; Daniels, A. D.; Farkas, Ö.; Foresman, J. B.; Ortiz, J. V.; Cioslowski, J.; Fox, D. J. *Gaussian 09*, Revision A.01; Gaussian, Inc., Wallingford CT, 2009.
(27) Roca-Sabio, A.; Regueiro-Figueroa, M.; Esteban-Gomez, D.; de Blas, A.; Rodriguez-Blas, T.; Platas-Iglesias, C. *Comput. Theo. Chem.* **2012**, *999*, 93−104.
(28) Esteban-Gomez, D.; de Blas, A.; Rodriguez-Blas, T.; Helm, L.; Platas-Iglesias, C. *ChemPhysChem* **2012**, *13*, 3640−3650.
(29) Dolg, M.; Stoll, H.; Savin, A.; Preuss, H. *Theor. Chim. Acta* **1989**, *75*, 173−194.
(30) (a) Maron, L.; Eisenstein, O. *J. Phys. Chem. A* **2000**, *104*, 7140−7143. (b) Eisenstein, O.; Maron, L. *J. Organomet. Chem.* **2002**, *647*, 190−197.
(31) Platas-Iglesias, C.; Roca-Sabio, A.; Regueiro-Figueroa, M.; Esteban-Gómez, D.; de Blas, A.; Rodríguez-Blas, T. *Current Inorg. Chem.* **2011**, *1*, 91−116.
(32) Platas-Iglesias, C. *Eur. J. Inorg. Chem.* **2005**, *105*, 2023−2033.
(33) (a) Peng, C.; Ayala, P. Y.; Schlegel, H. B.; Frisch, M. J. *J. Comput. Chem.* **1996**, *17*, 49−56. (b) Peng, C.; Schlegel, H. B. *Isr. J. Chem.* **1994**, *33*, 449−454.
(34) Tomasi, J.; Mennucci, B.; Cammi, R. *Chem. Rev.* **2005**, *105*, 2999−3093.
(35) Gill, N. S.; Nuttall, R. H.; Scaife, D. E.; Sharp, D. W. *J. Inorg. Nucl. Chem.* **1961**, *18*, 79−87.
(36) Carnall, W. T.; Siegel, S.; Ferraro, J. R.; Tani, B.; Gebert, E. *Inorg. Chem.* **1973**, *12*, 560−564.
(37) Sim, L. N.; Majid, S. R.; Arof, A. K. *Vibr. Spectrosc.* **2012**, *58*, 57.
(38) (a) Valencia, L.; Martínez, J.; Macías, A.; Bastida, R.; Carvalho, R. A.; Geraldes, C. F. G. C. *Inorg. Chem.* **2002**, *41*, 5300−5312. (b) Fernández-Fernández, M.; del, C.; Bastida, R.; Macías, A.; Pérez-Lourido, P.; Platas-Iglesias, C.; Valencia, L. *Inorg. Chem* **2006**, *45*, 4484−4496. (c) Núñez, C.; Mato-Iglesias, M.; Bastida, R.; Macías, A.; Pérez-Lourido, P.; Platas-Iglesias, C.; Valencia, L. *Eur. J. Inorg. Chem.* **2009**, 1086−1095.
(39) Seitz, M.; Oliver, A. G.; Raymond, K. N. *J. Am. Chem. Soc.* **2007**, *129*, 11153−11160.
(40) (a) Hunter, C. A.; Sanders, J. K. M. *J. Am. Chem. Soc.* **1990**, *112*, 5525−5534. (b) Song, R.-F.; Xie, Y.-B.; Li, J.-R.; Bu, X.-H. *Dalton Trans.* **2003**, 4742−4748.
(41) Platas, C.; Avecilla, F.; de Blas, A.; Rodríguez-Blas, T.; Geraldes, C. F. G. C.; Coth, E.; Merbach, A. E.; Bunzli, J.-C. G. *J. Chem. Soc., Dalton Trans.* **2000**, 611−618.
(42) Peters, J. A.; Huskens, J.; Raber, D. J. *Prog. NMR Spectrosc.* **1996**, *28*, 283−350.
(43) Bleaney, B. *J. Magn. Reson.* **1972**, *8*, 91−100.
(44) (a) Cosentino, U.; Villa, A.; Pitea, D.; Moro, G.; Barone, V.; Maiocchi, A. *J. Am. Chem. Soc.* **2002**, *124*, 4901−4909. (b) Purgel, M.; Baranyai, Z.; Blas, A.; Rodríguez-Blas, T.; Bányai, I.; Platas-Iglesias, C.; Tóth, I. *Inorg. Chem.* **2010**, *49*, 4370−4382. (c) Di Vaira, M.; Stoppioni, P. *New J. Chem.* **2002**, *26*, 136. (d) Regueiro-Figueroa, M.; Esteban-Gómez, D.; de Blas, A.; Rodríguez-Blas, T.; Platas-Iglesias, C. *Eur. J. Inorg. Chem.* **2010**, 3586−3595.
(45) (a) Natrajan, L. S.; Khoabane, N. M.; Dadds, B. L.; Muryn, C. A.; Pritchard, R. G.; Heath, S. L.; Kenwright, A. M.; Kuprov, I.; Faulkner, S. *Inorg. Chem.* **2010**, *49*, 7700−7709. (b) Dunand, F. A.; Dickins, R. S.; Parker, D.; Merbach, A. E. *Chem.—Eur. J.* **2001**, *7*, 5160−5167. (c) Aime, S.; Barge, A.; Botta, M.; Fasano, M.; Ayala, J. D.; Bombieri, G. *Inorg. Chim. Acta* **1996**, *246*, 423−429.
(46) Platas-Iglesias, C. *Eur. J. Inorg. Chem.* **2012**, 2023−2033.
(47) (a) Liang, X.; Weishäupl, M.; Parkinson, J. A.; Parsons, S.; McGregor, P. A.; Sadler, P. J. *Chem.—Eur. J.* **2003**, *9*, 4709−4717. (b) Buckingham, D. A.; Clark, C. R.; Rogers, A. J. *J. Am. Chem. Soc.* **1997**, *119*, 4050−4058.